# Supplementary Information: First-principles momentum distributions and vibrationally corrected permittivities of hexagonal and cubic ice

Edgar A. Engel, Irene Li, and Richard J. Needs
*TCM Group, Cavendish Laboratory, J J Thomson Avenue, Cambridge, CB3 0HE, UK*

## I. TEMPERATURE AND PRESSURE DEPENDENCE

Fig. S1 (a) shows the spherically-averaged $n_p(p)$ for temperatures ranging from 0 K to 5000 K in order to demonstrate that at sufficiently high temperatures the increasing thermal motion of the protons becomes comparable in size to their quantum ZP motion and is reflected in $n_p(p)$. In practice ice melts at about 273 K, at which point $n_p(p)$ is indistinguishable from its 0 K counterpart. Figs. S1 (a) and (c) show the projection of single proton and the proton-averaged $n(\mathbf{p})$ at 0 K and 268 K onto the (001) plane, respectively. While the proton-averaged $n(\mathbf{p})$ at 0 K and 268 K are indistinguishable, Fig. S1 (b) suggests a weak temperature dependence of $n(\mathbf{p})$ of an individual proton along the direction orthogonal to the O–H covalent bond. However, on the scale of the effects of stacking-disorder and vibrational anharmonicity neither the proton-averaged $n(\mathbf{p})$ nor the $n(\mathbf{p})$ of an individual proton exhibit a significant temperature dependence.

Figs. S2 (a) to (c) show the absence of a significant pressure dependence of $n(\mathbf{p})$ up to the Ih–II and Ih–III transitions pressures, despite the volume changes of up to around 2% collected in Table S1. The anharmonic correction to the vibrational free energy of Ih increases by about 0.2 meV/$H_2O$ or, equivalently, about 4 %. Crucially, the softening of pseudo-translations and librational modes leads to a decrease in harmonic vibrational free energy under pressure, leaving the total vibrational free energy essentially unchanged under pressure – similarly to the proton kinetic energy.

| $P$ [MPa] | $c$ [Å] | V [Å$^3$/$H_2O$] | $\Delta u_{\mathrm{RMS,anh}}$ [Å] |
|---|---|---|---|
| -100 | 7.11 | 29.35 | 0.4016(6) |
| 0 | 7.10 | 29.29 | 0.4010(6) |
| 100 | 7.08 | 28.98 | 0.4008(6) |
| 200 | 7.06 | 28.81 | 0.4005(6) |

TABLE S1. Dependence on pressure, $P$, of unit cell parameters and proton RMS displacements in ice Ih $Cmc2_1$, $\Delta u_{\mathrm{RMS}}$.

## II. DEPENDENCE OF $Z^*$ ON VIBRATIONAL DISPLACEMENTS

In order to understand why the nuclear polarisability of ice is affected by nuclear motion it is necessesary to understand how the Born effective charges $Z^*_{\alpha\beta}$ associated with a particular atom depend on general vibrational displacements $\mathbf{q}$. To gain an atomistic insight we decompose $Z^*_{\alpha\beta}$ into an equilibrium/static-lattice term $Z^{*(0)}_{\alpha\beta}$, independent-mode terms $Z^{*(1)}_{\alpha\beta}(q_i)$, pair terms $Z^{*(2)}_{\alpha\beta}(q_i, q_j)$, etc,:

$$\begin{aligned} Z^*_{\alpha\beta}(\mathbf{q}) &= Z^{*(0)}_{\alpha\beta} + \sum_i Z^{*(1)}_{\alpha\beta}(q_i) + \sum_{i,j} Z^{*(2)}_{\alpha\beta}(q_i, q_j) + \dots \\ Z^{*(0)}_{\alpha\beta} &\equiv Z^*_{\alpha\beta}(\mathbf{q} = \mathbf{0}) \\ Z^{*(1)}_{\alpha\beta}(q_i) &\equiv Z^*_{\alpha\beta}(q_i\,, q_{j\neq i} = 0) - Z^{*(0)}_{\alpha\beta} \\ Z^{*(2)}_{\alpha\beta}(q_i, q_j) &\equiv Z^{*(2)}_{\alpha\beta}(q_i\,, q_j\,, q_{k\neq i,j} = 0) \\ &\quad - Z^{*(0)}_{\alpha\beta} - Z^{*(1)}_{\alpha\beta}(q_i) - Z^{*(1)}_{\alpha\beta}(q_j) \end{aligned} \tag{1}$$

$Z^{*(1)}_{\alpha\beta}(q_i)$ is typically dominated by a linear dependence on $q_i$ as illustrated in Fig. S4 (a). However, this linear dependence does not contribute to the vibrationally corrected $Z^*_{\alpha\beta}$ due to the symmetry of the vibrational wavefunction. Fig. S4 (b) shows the less common case, in which $Z^{*(1)}_{\alpha\beta}(q_i)$ clearly involves higher order (even) terms in $q_i$, which contribute to the vibrationally corrected $Z^*_{\alpha\beta}$.

Fig. S4 (c) shows a particular pairwise term $Z^{*(2)}_{\alpha\beta}(q_i, q_j)$. It is small in comparison to the independent mode terms $Z^{*(1)}_{\alpha\beta}(q_i)$ and antisymmetric, so that its contribution to the vibrationally corrected $Z^*_{\alpha\beta}$ is negligible, suggesting that pairwise terms do not play a significant role. Nonetheless the vibrationally corrected $Z^*_{\alpha\beta}$ in the main text were evaluated using a Monte Carlo sampling approach in which the vibrationally corrected $Z^*_{\alpha\beta}$ are evaluated as the mean

$$\overline{Z^*_{\alpha\beta}} = \frac{1}{N}\sum_{i=1}^{N} Z^*_{\alpha\beta}(\mathbf{q}_i) \tag{2}$$

over $N$ frozen-phonon configurations $\mathbf{q}_i$, which are drawn from the harmonic vibrational density as the underlying probability distribution and for each of which an individual PBE-DFT calculation was performed to determine $Z^*_{\alpha\beta}(\mathbf{q}_i)$. This approach accounts for the full dependence of $Z^*_{\alpha\beta}(\mathbf{q})$ on $\mathbf{q}$.

## III. PERMITTIVITY OF DIFFERENT IH PROTON-ORDERINGS

Fig. S6 shows $\epsilon$ for the 16 eight-molecule proton-orderings of Hirsch and Ojamae [1]. The permittivity

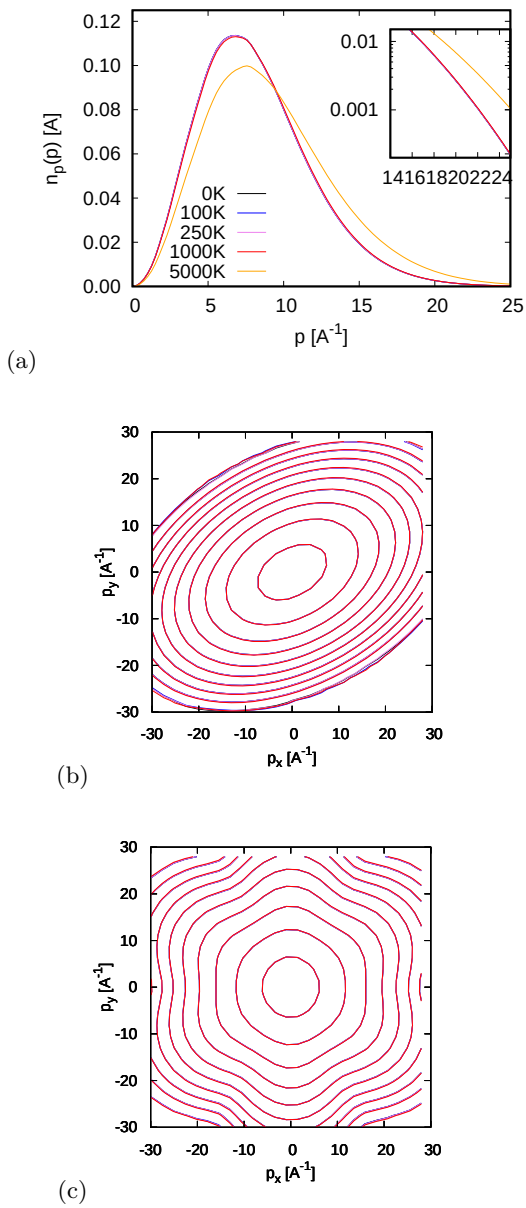


FIG. S1. Temperature dependence of (a) the spherically-averaged MDF and the projection of the spatially-resolved MDF of (b) a single proton and (c) averaged over all protons in Ih $Cmc2_1$ onto the (001) plane up to unphysically high temperatures. Up to the melting point thermal effects are negligible.

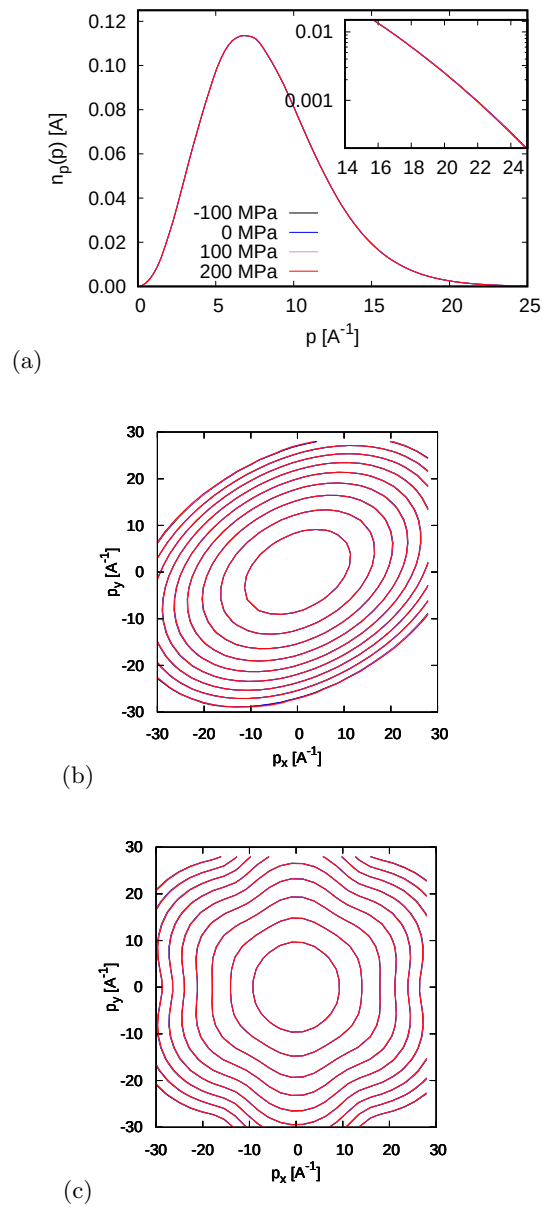


FIG. S2. Pressure dependence of (a) the spherically-averaged and the projection of the spatially-resolved MDF of (b) a single proton and (c) averaged over all protons in Ih $Cmc2_1$ onto the (001) plane up to the Ih–II and Ih–III transition pressures.

$\epsilon$ in the Mhz-range depends sensitively on the particular proton-ordering and varies by up to 14% between proton-orderings. In contrast, the vibrational corrections to $\epsilon$ are very similar for all proton-orderings and are larger than 5% of the static-lattice value in all cases considered.

The details regarding the symmetries groups of the 16 eight-molecule proton-orderings and their static-lattice $E^i_{\text{static}}$ and vibrationally corrected configurational energies $E^i$, etc. are collected in Table S2.

## IV. ROLE OF THE $xc$-FUNCTIONAL

Semi-local generalised gradient approximations such as the PBE [2], optPBE [3], and WC [4] functionals shown in Fig. S5 (a) all produce very similar values for $\epsilon$. However, in general the static-lattice and, in consequence, the vibrationally corrected $\epsilon$ of ice depends substantially on the choice of $xc$-functional. For example, the hybrid HSE06 functional [5–7] produces a static-lattice $\epsilon$ of 2.61, while the LDA [8–10] results in a value of 3.06. However, these large differences between functionals arise predominantly

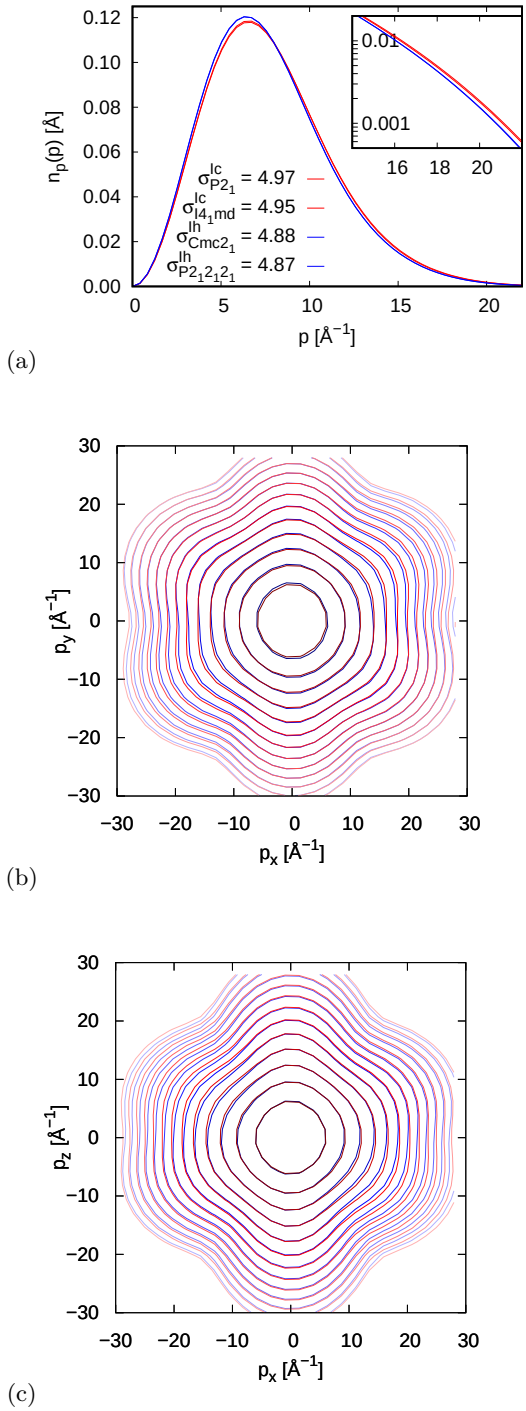


FIG. S3. Dependence on stacking and proton-order of (a) the spherically-averaged and the projection of the proton-averaged spatially-resolved MDF of Ih $Cmc2_1$ and $P2_12_12_1$, and Ic $I4_1md$ and $P2_1$ onto the (b) basal and (c) prism plane, respectively.

| i | Space group | $E^i_{\text{static}}$ | $\Delta E^i_{\text{har}}$ | $\Delta E^i_{\text{anh}}$ | $E^i$ |
|---|---|---|---|---|---|
| 1 | $Cc$ | 1.02 | -0.62 | 6.42 | 7.01 |
| 2 | $Cmc2_1$ | 0.00 | 0.00 | 6.97 | 6.97 |
| 3 | $P1$ | 1.17 | -0.06 | 6.73 | 7.84 |
| 4 | $Pc$ | 1.83 | -0.21 | 7.65 | 9.26 |
| 5 | $P2_1$ | 4.00 | -0.72 | 7.00 | 10.27 |
| 6 | $P2_1$ | 3.98 | -0.71 | 6.65 | 9.92 |
| 7 | $P2_1$ | 1.32 | -0.19 | 7.32 | 8.45 |
| 8 | $P2_1$ | 2.39 | -0.92 | 7.16 | 8.63 |
| 9 | $Pc$ | 1.72 | -0.19 | 8.34 | 9.86 |
| 10 | $Pc$ | 2.39 | -0.69 | 6.76 | 8.45 |
| 11 | $P2_12_12_1$ | 5.18 | -0.79 | 6.44 | 10.83 |
| 12 | $P2_12_12_1$ | 2.77 | -0.52 | 6.28 | 8.53 |
| 13 | $Pbn2_1$ | 2.35 | -0.30 | 5.96 | 8.01 |
| 14 | $Pca2_1$ | 1.34 | -0.13 | 5.58 | 6.99 |
| 15 | $Pna2_1$ | 4.16 | -0.88 | 6.42 | 9.69 |
| 16 | $Pna2_1$ | 3.83 | -0.59 | 6.26 | 9.50 |

TABLE S2. Space groups, static-lattice energies $E^i_{\text{static}}$, harmonic lattice free energies $\Delta E^i_{\text{har}}$, and anharmonic corrections $\Delta E^i_{\text{anh}}$, at 0 K for the 16 Ih proton-orderings of Hirsch and Ojamae [1]. All energies are measured in meV/$H_2O$. $E^i_{\text{static}}$ and $\Delta E^i_{\text{har}}$ are measured relative to the values for Ih $Cmc2_1$ (also referred to as XIh). For Ih $Cmc2_1$ $\Delta E^2_{\text{har}}$ = 692.34 meV/$H_2O$.

from the different unit cell volumes arising from geometry optimisation with the respective $xc$-functionals. Setting aside results obtained with the LDA, fixing the unit cell parameters to the experimental values renders the static-lattice $\epsilon$ and the vibrational properties (and therefore the vibrational correction to $\epsilon$) insensitive to the choice of $xc$-functional (see Fig. S5 (a)).

Fig. S5 (b) shows the convergence of the harmonic and anharmonic Monte Carlo sampled vibrationally corrected $\epsilon$ of Ih $Cmc2_1$ obtained using different $xc$-functionals (but the same PBE frozen-phonon configurations) with the number of frozen-phonon configurations sampled.

Fig. S5 (c) shows the dependence of the temperature dependent vibrational correction to $\epsilon$ of Ih $Cmc2_1$ obtained using the PBE functional with and without Tkatschenko-Scheffler (TS) dispersion correction [11]. Here the sampled frozen-phonon configurations were constructed using PBE and PBE-TS optimised unit cells and vibrational data, respectively. The differences in the vibrational correction to $\epsilon$ arise predominantly from the different unit cell volumes and the resulting different vibrational properties obtained with and without the TS dispersion correction.

[1] K. Hirsch and L. Ojamäe, Quantum-chemical and force-field investigations of ice Ih: computation of proton-ordered structures and prediction of their lattice energies, *Journal of Physical Chemistry B* **108**, 15856 (2004).

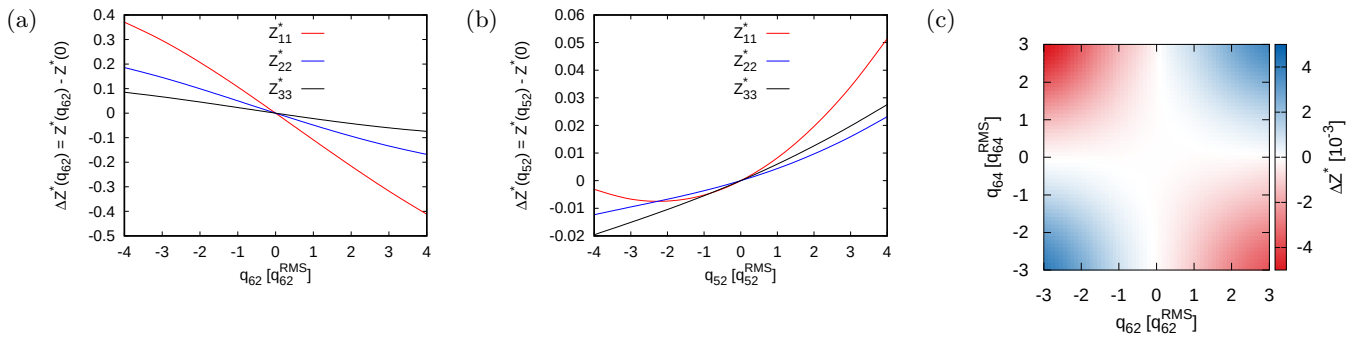


FIG. S4. (a) Typical strong linear dependence of the diagonal elements of $Z^*_{ij}(q)$ on the vibrational displacement, $q$, along a particular mode. However, linear terms cancel when integrated over the symmetric vibrational wavefunction and therefore do not contribute to the vibrational renormalisation of $Z^*$. (b) The quadratic dependence of $Z^*_{11}(q)$ leads to vibrational renormalisation of $Z^*_{11}$ for the symmetric vibrational wavefunction. (c) Even the largest corrections from cross-terms, $q_i^n q_j^m$, are generally negligible and typically do not contribute to the vibrational renormalisation of $Z^*$ due to the symmetry of the vibrational wavefunction.

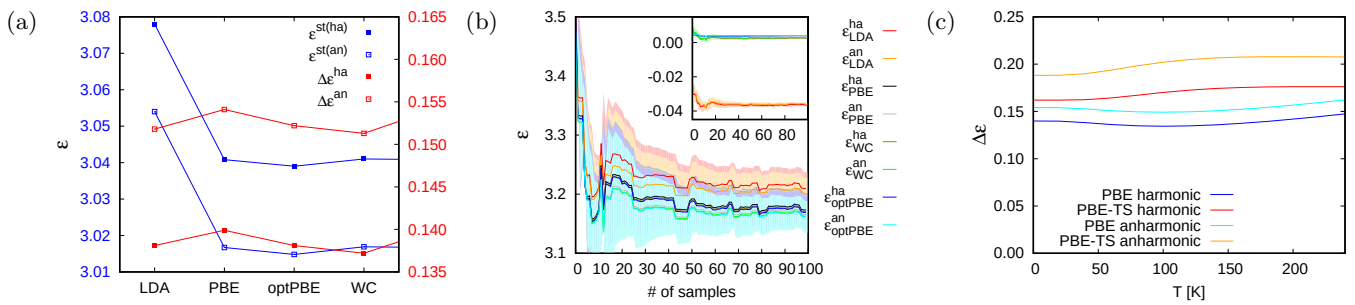


FIG. S5. (a) Dependence of the static-lattice and vibrationally corrected ZP $\epsilon$ on the choice of $xc$-functional for the same set of PBE-DFT frozen-phonon configurations. (b) Convergence of the absolute and relative vibrationally corrected ZP $\epsilon$ with the number of frozen-phonon samples for different $xc$-functionals. (c) Temperature dependence of $\epsilon$ using PBE and PBE-TS frozen-phonon configurations, respectively.

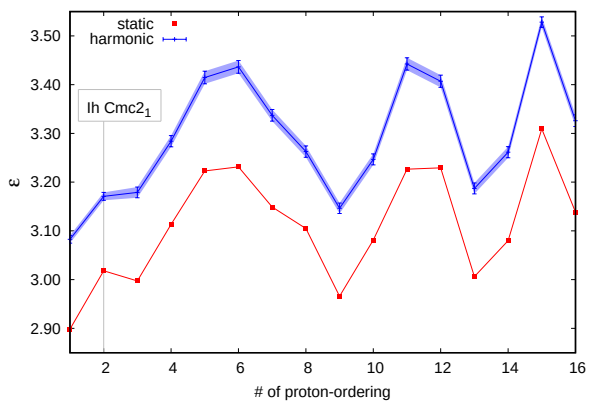


FIG. S6. Dependence on proton order of the static-lattice $\epsilon$ and $\epsilon$ in the harmonic approximation.


[2] J. P. Perdew, K. Burke, and M. Ernzerhof, Generalized Gradient Approximation Made Simple, *Physical Review Letters* **77**, 3865 (1996).

[3] J. Klimeš, D. R. Bowler, and A. Michaelides, Chemical accuracy for the van der Waals density functional, *Journal of Physics: Condensed Matter* **22**, 022201 (2009).

[4] Z. Wu and R. E. Cohen, More accurate generalized gradient approximation for solids, *Physical Review B* **73**, 235116 (2006).

[5] J. Heyd, G. Scuseria, and M. Ernzerhof, Hybrid functionals based on a screened Coulomb potential, *Journal of Chemical Physics* **118**, 8207 (2003).

[6] J. Heyd, G. Scuseria, and M. Ernzerhof, Erratum: "Hybrid functionals based on a screened Coulomb potential", *Journal of Chemical Physics* **124**, 219901 (2006).

[7] J. Paier, M. Marsman, K. Hummer, G. Kresse, I. C. Gerber, and J. G. Ángyán, Screened hybrid density functionals applied to solids, *Journal of Chemical Physics* **124**, 154709 (2006).

[8] D. M. Ceperley and B. J. Alder, Ground State of the Electron Gas by a Stochastic Method, *Physical Review Letters* **45**, 566 (1980).

[9] J. P. Perdew and A. Zunger, Self-interaction correction to density-functional approximations for many-electron systems, *Physical Review B* **23**, 5048 (1981).

[10] J. P. Perdew and Y. Wang, Accurate and simple analytic representation of the electron-gas correlation energy, *Physical Review B* **45**, 13244 (1992).

[11] A. Tkatchenko and M. Scheffler, Accurate Molecular Van Der Waals Interactions from Ground-State Electron Den-

sity and Free-Atom Reference Data, *Physical Review Letters* **102**, 073005 (2009).